Bulletin of the Seismological Society of America, Vol. 107, No. 5, pp. 2525–2531, October 2017, doi: 10.1785/0120170004

Ⓔ

Short Note

Earthquake Source Mechanism and Rupture Directivity of the 12 September 2016 M_w 5.5 Gyeongju, South Korea, Earthquake

by YoungHee Kim, XiaoHui He, SiDao Ni, Hobin Lim, and Sun-Cheon Park

Abstract Two earthquakes (M_w 5.1 and 5.5) ruptured branches of the Yangsan fault system in Gyeongju, South Korea, on 12 September 2016. Aftershocks, including a notable M_w 4.3 earthquake on 19 September 2016, were clustered around the epicenters of the first two events. The M_w 5.5 earthquake is considered the largest earthquake in South Korea to have occurred during the modern instrumental recording period since 1978. Although there is no apparent surface rupture, these earthquakes have greatly shaken South Korea, leaving both physical and societal impacts. In this study, we determine the source mechanism and rupture directivity using regional seismic-waveform data to understand the earthquake source processes. Based on the waveform inversion, we report that the mainshock (M_w 5.5 event) is a strike-slip event with two nodal planes 117°/84°/21° and 24°/69°/173° at a depth of 14 km. The inversion also demonstrates that the mainshock event ruptured against the 24° seismogenic fault plane to the south-southwest, with a rupture length of ~4.3 km. This rupture propagation direction agrees well with the spatial distribution of relocated aftershock events and reported seismic intensities.

Electronic Supplement: Tables of earthquake source parameters and figures of station and event locations, velocity model, waveform fits, and relative misfit errors and optimal source mechanisms.

Introduction

At 10:44:32 UTC and 11:32:55 UTC on 12 September 2016, M_w 5.1 and 5.5 earthquakes occurred approximately one hour apart in the city of Gyeongju, South Korea (Fig. 1), and were felt even in the capital city, Seoul, more than 300 km to the northwest. Aftershocks, including a notable M_w 4.3 earthquake on September 19 at 11:33:58 UTC, were clustered around the epicenters of the first two events (Fig. 1). These earthquake activities were considered to have occurred in the Yangsan fault system, an interrelated system of the north-northeast–south-southwest-trending Yangsan fault and its splay faults (Kim *et al.*, 2016). Parts of the city suffered small-to-moderate damage in building structures, but no fatalities due to the sudden ground shaking were reported. Although no surface ruptures were reported for the events, the occurrence of the 2016 Gyeongju earthquakes invoked a re-examination of the previously held consensus regarding the activities of the fault system.

The M_w 5.5 earthquake is considered the largest earthquake in South Korea and the surrounding ocean floor to have occurred during the modern instrumental recording period since 1978. From A.D. 2 to 1989, more than 500 events occurred in the southeastern part of the Korean Peninsula, with at least 126 earthquakes in close proximity to the Yangsan fault system (Lee and Jin, 1991). Among the 126 events, at least 10 earthquakes of modified Mercalli intensity (MMI) scale exceeding VIII are considered to have occurred in Gyeongju, presumably related to the activity of the Yangsan fault system, based on historical literature documents (Lee and Jin, 1991). Although these historical earthquake data motivate paleoseismic investigations of the Yangsan fault system, difficulties related to the identification of fault-related deformation features over the past 2000 years arise, particularly in active zones where surface deformation due to fault slip competes with erosional processes (Jeong and Cheong, 2005). Figure 1b shows previous seismic activities, including the M_L 4.2 earthquake on 26 June 1997, which was considered to be the largest in Gyeongju during the instrumental period up to that time.

The north-northeast-trending Yangsan fault system (Fig. 1b) is a dominantly right-lateral strike-slip fault with

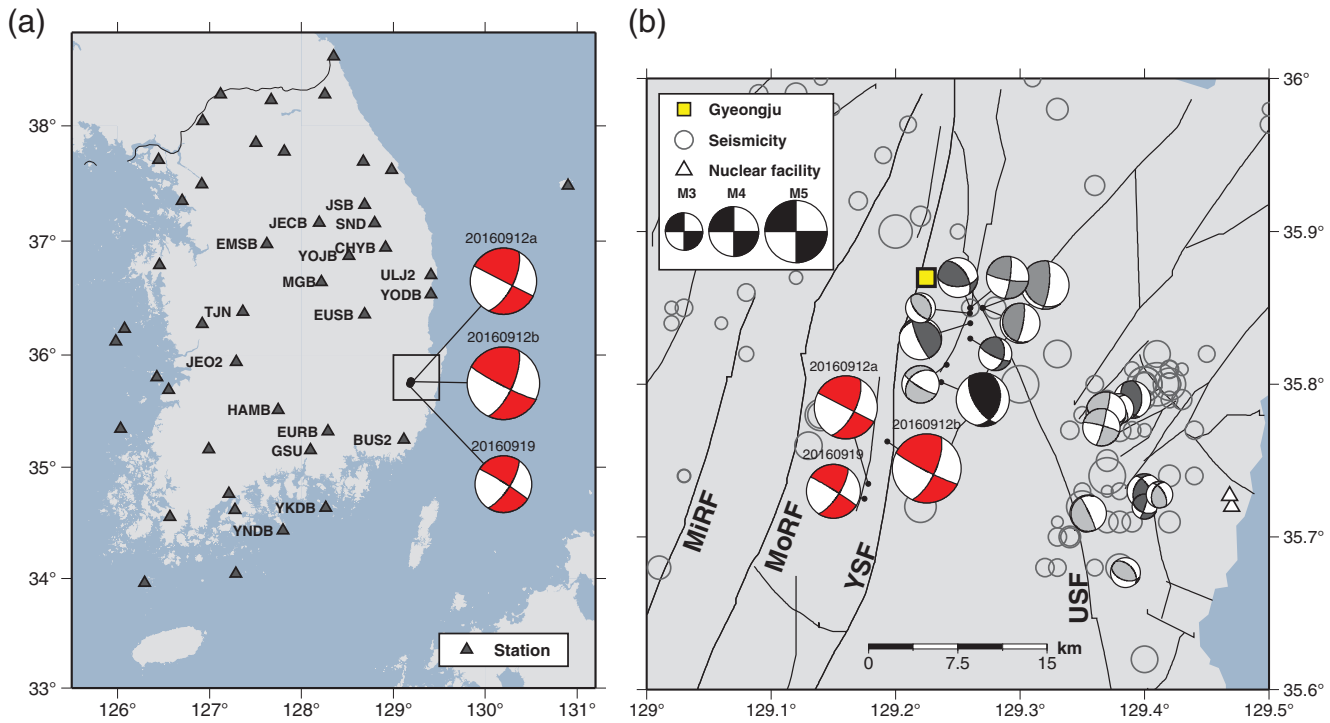

Figure 1. Regional seismotectonic setting of the 2016 Gyeongju earthquakes. (a) The seismic stations and the three earthquakes used in the analysis. The velocity sensors of epicentral distances within 200 km from the mainshock are shown with ID. (b) Earthquake source region. Black lines denote the lineaments and faults, with abbreviations YSF, Yangsan fault; MoRF, Moryang fault; MiRF, Miryang fault; USF, Ulsan fault. Previous seismicity during 2000–2016 is shown as gray open circles. Red focal mechanism plots with the date labeled show the source mechanisms of the 2016 Gyeongju events (20160912a for M_w 5.1 earthquake, 20160912b for M_w 5.5 earthquake, and 20160919 for M_w 4.3 earthquake). Other colored focal mechanism plots show past earthquakes (black, Chung and Kim, 2000; light gray, Chang *et al.*, 2010; medium gray, Jo and Baag, 2003; dark gray, Park *et al.*, 2007). The 26 June 1997 M_L 4.2 earthquake is shown as a black focal mechanism plot. Triangles represent the location of a nuclear dumpsite and nuclear power station.

a continuous trace ~200 km long (Kyung and Lee, 2006, and references therein). There are also other locally prominent lineament features in the north-northwest–west-northwest direction which dissects the north-northeast-trending Yangsan fault at several places (Um *et al.*, 1983). Both the northern and southern portions of the Yangsan fault system are believed to have been active during the late Quaternary period, based on limited fault-trench data (Kyung and Lee, 2006, and references therein).

The 2016 Gyeongju events prompt concerns over the safety of nuclear plants clustered in the earthquake source region. There are two critical infrastructures, including a nuclear waste disposal site and a nuclear power station, located just 27 km away from the epicenter of the M_w 5.5 event (Fig. 1b). These structures are designed to withstand earthquakes up to M_L 6.5 (0.2g), according to the Nuclear Safety and Security Commission. Regardless of seismic activities along the fault system, additional nuclear power plants are planned to be constructed, and thus there will be a total of 16 nuclear power plant units around the Yangsan fault system by 2021.

The 2016 Gyeongju earthquake activities clearly reflect a hidden intricate fault network and various processes in the Yangsan fault system. Thus, the determination of their accurate source parameters is of the utmost importance for understanding local seismic risks and associated tectonic activities. Using broadband waveform data from the regional seismic network in South Korea, we first examine the physical behavior of earthquake rupturing in the fault system because earthquake-source directivity is one of the key factors that affects ground shaking. For this, we adopt the method to constrain the rupture directivity proposed by Qin *et al.* (2014) and He *et al.* (2015), which is suitable for applying to a region where the seismic network is sparse and/or where accurate velocity models are not available. Also, we relocate aftershock earthquakes that occurred between 12 September and 15 November to delineate the rupture zone of the 2016 Gyeongju events.

Data and Method

For determining the source parameters of the three Gyeongju earthquakes that occurred on September 2016 (Fig. 1; 20160912a for M_w 5.1 earthquake [foreshock], 20160912b for M_w 5.5 earthquake [mainshock], and 20160919 for M_w 4.3 earthquake [the largest aftershock, hereafter, aftershock in this section]), we collect seismograms recorded from a total of 44 stations operated by the

Table 1
Earthquake Source Parameters of the 2016 September Gyeongju Earthquakes

Event ID (yyyymmdd)	Origin Time (UTC) (hh:mm:ss.ss)	Longitude (°E)	Latitude (°N)	Depth (km)	M_w	Strike (°)	Dip (°)	Rake (°)
20160912a	10:44:33.30	129.1780	35.7350	14.0	5.05	297; 27	90; 60	−24; −180
20160912b	11:32:54.80	129.1932	35.7628	14.0	5.54	117; 24	84; 69	21; 173
20160919	11:33:59.26	129.1750	35.7250	16.0	4.32	302; 33	86; 72	−18; −175

seismic network of the Korea Meteorological Administration [KMA] and the Korea Institute of Geoscience and Mineral Resource (Ⓔ Fig. S1, available in the electronic supplement to this article). To constrain the source mechanism and the rupture directivity, we follow the inversion procedure by Qin *et al.* (2014) and He *et al.* (2015), which we briefly describe in the context of how we apply it to the Korean seismic data.

There are three steps for determining source parameters. First, we relocate the relative hypocenters of the foreshock and aftershock events with the relative *P*- and *S*-wave onset at three nearest stations (within 100 km from the mainshock), based on HYPO2000 (Klein, 2002). Second, we calculate the Green's function from the frequency–wavenumber (f-k) method (Zhu and Rivera, 2002), using a 1D velocity model (Kim *et al.*, 2011; Ⓔ Fig. S2) and obtain a point-source solution by inverting for focal mechanism and centroid depth with the waveform inversion method (called the cut-and-paste [CAP] method; Zhao and Helmberger, 1994). To account for inaccuracy in crustal models, Zhao and Helmberger (1994) partitioned three-component waveforms into body-wave and surface-wave segments and allowed independent time shifting for each of them. In total, five segments are used in the inversion, that is, the radial and vertical components of body waves (*P* wave and following multiples, *Pnl*) and the Rayleigh surface wave and the tangential component of the Love surface wave. The time window for the *Pnl* and surface wave is 20 and 60 s, respectively. During the inversion, body waves are filtered at 0.05–0.2 Hz for the mainshock, the foreshock, and the aftershock. Because surface waves are usually more coherent in the long period, a pass-band of 0.05–0.1 Hz is applied. But for the aftershock, the band-pass filter range of 0.05–0.2 Hz is used for the surface wave, because the synthetic seismograms match the observation very well up to 0.2 Hz.

Finally, we calculate the time-shift difference between the mainshock and the reference event and analyze its azimuthal variation and resolve the rupture plane by fitting it with the following equation:

$$dt = (T_{obs} - T_{syn})_A - (T_{obs} - T_{syn})_B = t_0 - (L/2V) \times \cos(az - stk), \quad (1)$$

in which dt is the time-shift difference between the mainshock and reference event; $T_{obs} - T_{syn}$ is the time shift between the observed data and the 1D synthetics from the CAP inversion; A is the mainshock, and B is the reference event; V is the apparent speed for different phases; az is the azimuth of the stations (defined for mainshock); stk is the strike for either of the nodal planes (NP) of the mainshock; t_0 is the source-time-duration difference between the mainshock and the reference event; L is the rupture length; and the +/− sign of L represents rupturing along or against the strike. By fitting observed data with the least-squares method, the NP with the smaller residual can be considered the seismogenic fault plane, and the rupture length is estimated simultaneously.

For relocating aftershocks, we collect a total of 158 aftershocks with $M_L < 3.5$ that occurred between 12 September (the time after the foreshock) and 15 November, recorded from the stations (Ⓔ Fig. S1) and use the earthquake catalog provided by KMA (which does not include focal depths). The hypocenters are determined with the program Baysian Hierarchical Seismic Event Locator (Bayesloc) (Myers *et al.*, 2007, 2009), based on manually picked 878 *Pg* arrival times and a velocity model (Ⓔ Fig. S2; Kim *et al.*, 2011) to minimize the uncertainty of the earthquake location determined by KMA. The Bayesloc samples join the probability density functions of the hypocenters of the multiple events with allowed errors of the arrival times and the velocity model (Myers *et al.*, 2007, 2009).

We exclude the aftershocks with large uncertainties in depth (larger than 1σ error, which exceeds 2.5 km) and finally obtain 102 aftershocks (which includes the largest aftershock, 20160919, in Table 1). We then calculate the relative locations of the 102 events with the program hypoDD (Waldhauser and Ellsworth, 2000). We select the aftershock 20160919 as a reference event and shift the aftershocks based on the reference-event location because hypoDD cannot provide the absolute location of the earthquakes. See Ⓔ Table S3 for the temporal and spatial shifts that occurred in each calculation step.

Source Parameters and Rupture Directivity of the Mainshock Event

The inversion results show that all three earthquakes show strike-slip motion that occurred at a focal depth of 14–16 km (Table 1; Fig. 2). The mainshock has a moment magnitude of 5.5, a focal depth of 14 km, and a duration of 2 s (Fig. 2). The two NPs are 117°/84°/21° (NP 1) and 24°/69°/173° (NP 2), consistent with the moment tensor inversion result (Kim *et al.*, 2016), Global Centroid Moment Tensor solution and the U.S. Geological Survey moment

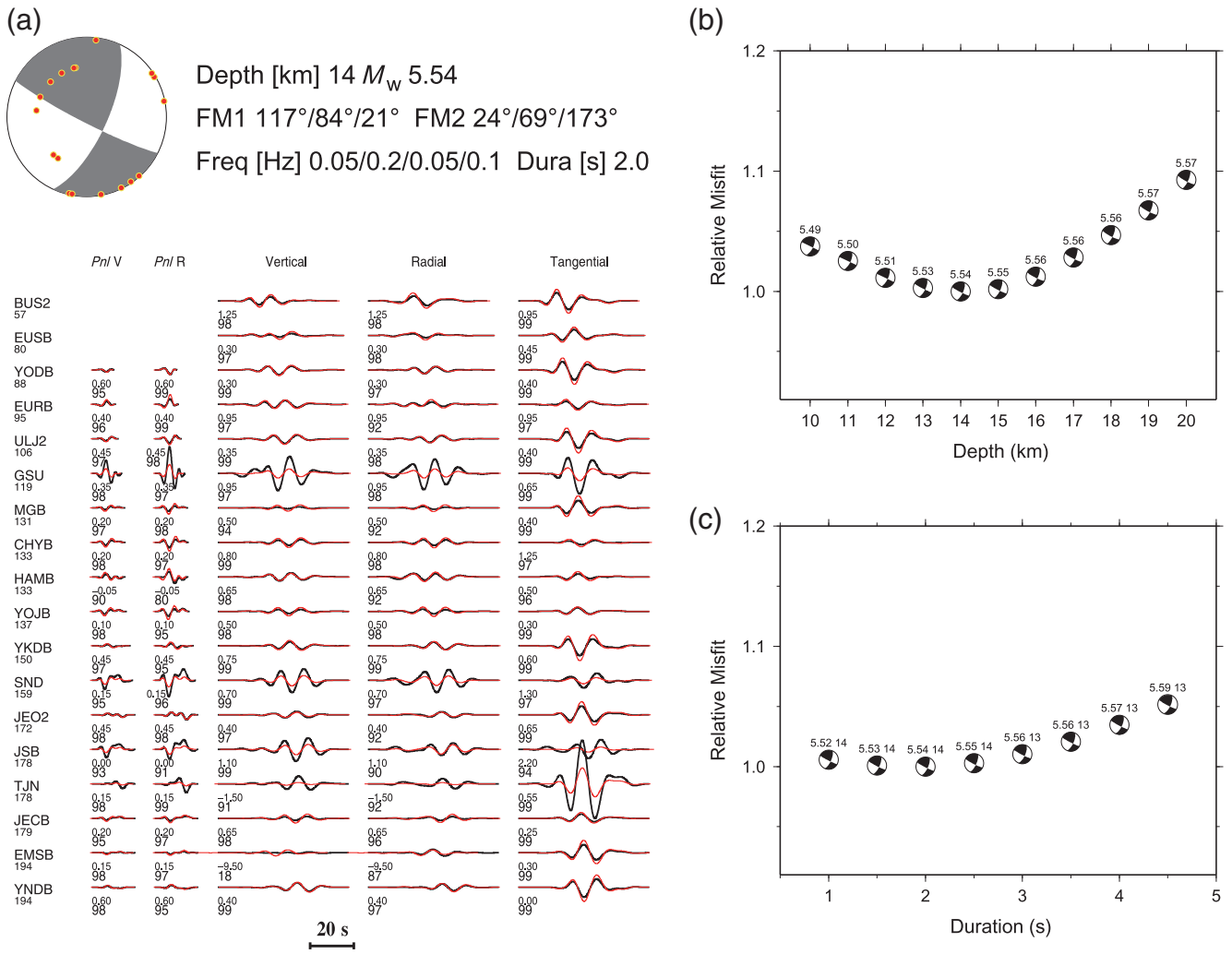

Figure 2. Source mechanism of the mainshock (M_w 5.5 event). (a) Cut-and-paste inversion results showing the focal mechanism and waveform fit between the synthetic (red) and observed (black) seismograms for *Pnl* and the surface wave. Numbers to the left of the seismograms are time shifts (upper numbers) and a cross-correlation coefficient in percent (lower numbers). The station ID (Fig. 1a) and epicentral distance are specified for each waveform fit. Note that all station data are displayed in Ⓔ Figure S1, available in the electronic supplement to this article. The plots for the foreshock (M_w 5.1 event) and aftershock (M_w 4.3 event) are displayed in Ⓔ Figures S4 and S5, respectively. (b) Relative misfit errors and optimal source mechanisms at each depth. Focal mechanism of each depth is indicated with the focal mechanism plot, and the number above the focal mechanism plot is the moment magnitude. (c) Relative misfit errors, optimal duration, and focal depth. The numbers above the focal mechanism plot are the moment magnitude and optimal focal depth.

tensor solution (Ⓔ Table S1). The observations fit well with the synthetics, with cross-correlation coefficients larger than 0.9 for most stations (Fig. 2 and Ⓔ Fig. S3). The foreshock event has a moment magnitude of 5.1 and a depth of 14 km, and the focal mechanism is similar to the mainshock with NPs 297°/90°/−24° (NP 1) and 27°/60°/−180° (NP 2) (Ⓔ Figs. S4 and S6a). The largest aftershock has a moment magnitude of 4.3 and a depth of 16 km, and the two NPs are 302°/86°/−18° (NP 1) and 33°/72°/−175° (NP 2) (Ⓔ Figs. S5 and S6b).

At local distances, a series of depth phases can be used to estimate focal depth, and they are mostly converted from upgoing *S* waves, including *sPg*, *sPmP*, *sPn* (Ma and Atkinson, 2006; Ma, 2010), and *sPL* (an *S* wave that goes upward and is postcritically converted to a *P* wave traveling along the free surface; Chong *et al.*, 2010). In particular, *sPL* develops at a short distance (<60 km) and gradually becomes *sPg* at larger distances (Ma and Atkinson, 2006). Though *Pn* is clear on many stations, *sPn* is difficult to identify, probably due to contamination of *Pg*. The *sPL* phase can be observed at an approximate distance of 50 km (e.g., station BUS2, 57 km) and *sPg* (e.g., station EURB, 95 km). The measured arrival-time difference between the depth phases and *P*-wave phases from the vertical-component displacement of stations BUS2 and EURB (Ⓔ Fig. S7) is about 3.6–4.1 s, which corresponds to about 10–13 km, based on the 1D model (Kim *et al.*, 2011). These values are roughly consistent with the focal depth estimates (14–16 km) by the CAP inversion.

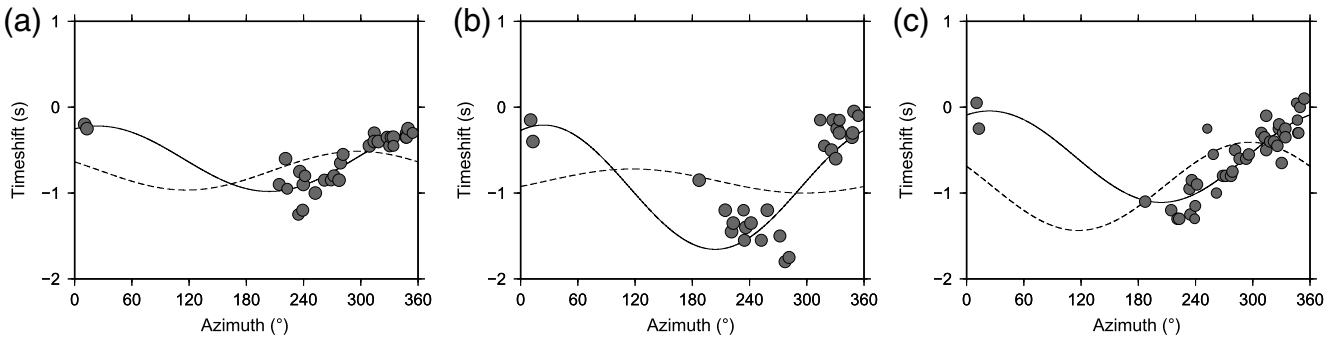

Figure 3. Differential time fitting with azimuth variation for (a) *Pnl*, (b) Rayleigh, and (c) Love waves. The time shift is estimated from equation (1), using the foreshock event as the reference event. The size of the circle is in proportion to the waveform cross-correlation coefficient, which is larger than 0.8. Solid and dashed lines represent the theoretic time shift for nodal planes striking 24° and 117°, respectively.

By fitting the time shift based on equation (1), using the M_w 5.1 foreshock as a reference event, we find that the time-shift difference data fit better when the strike is 24°. Furthermore, we obtain a negative fault rupture length, for which negative rupture means the rupture that propagates to the opposite direction against the fault plane. Thus, our analysis results suggest that the mainshock ruptured against the 24° NP to the south-southwest (Fig. 3). The resolved rupture length is 4.6 km (constrained from *Pnl*), 4.5 km (Rayleigh wave), and 3.7 km (Love wave) (Table 2), and the mean value of the three rupture lengths is 4.3 km. Following a similar procedure and using the M_w 4.3 aftershock as a reference, we also find that the time-shift difference data fit better when the strike is 24° (Ⓔ Fig. S8), regardless of using much less station data in the fitting, due to a lower signal-to-noise ratio of the aftershock event. The resolved rupture length is 3.5 km (constrained from *Pnl*), 2.2 km (Rayleigh wave), and 4.1 km (Love wave), with a mean value of 3.3 km (Ⓔ Table S2).

Fault Geometry Constrained by Relocated Aftershocks and Seismic Intensities in Relation with the Rupture Direction

The relocated aftershock events based on the double-difference algorithm (Waldhauser and Ellsworth, 2000) for a period of about two months are shown in Figure 4a. The relocation of the aftershocks with M_L 2.0–3.5 illuminates the spatial extent of a fault rupture zone within the Yangsan fault system. The spatial distribution of the aftershocks is consistent with the along-strike rupture propagation of the mainshock (~24° fault plane) to the south-southwest on the fault system (Fig. 4a). The events occur at the focal depth range of 10–18 km, with the highest seismic activity at a depth of 14 km (Fig. 4b,d,e).

Table 2
Rupture Directivity Estimation Result with Foreshock (20160912a) as Reference Event

Phase	Number of Stations	NP1 Misfit (Strike = 117°)	NP2 Misfit (Strike = 24°)	Rupture Length (km)
Pnl	32	0.29	0.13	4.6
Rayleigh	30	0.76	0.56	4.5
Love	43	0.37	0.19	3.7

NP, nodal plane.

Figure 4c shows the map of the MMI intensity estimates (the scale V–VIII), provided by KMA (9.12 Earthquake Survey and Response Team of KMA). The MMI values are based on reported damages surveyed by local governments. We observe that the MMI VII and VIII intensities are dominantly reported along the north-northeast–south-southwest-trending Yangsan fault system between the latitude of 35.6° and 36.0° (navy- and green-colored dots shown in Fig. 4c). Comparing the same dimension (20 km × 30 km) to the northeast and southwest direction from the epicenter, the ratios of the number of MMI VII and VIII intensities to that of MMI V–VIII are 0.9% to the northeast and 4.0% to the southwest, respectively. In particular, two sites report high-intensity estimates (MMI VIII), which are all located southwest of the focal area (green colored dots shown in Fig. 4c). This is roughly in agreement with the rupture propagation direction. The sites with the most damage reported are in a high elevation compared to the city of Gyeongju (Ⓔ Figs. S9d and S10) and involve Late Cretaceous to Early Tertiary igneous rocks and Late Mesozoic Yucheon volcanics (Kyung, 2003). Late Mesozoic Kyongsang basin deposits are mostly present in the east of the Yangsan fault (Kyung, 2003). Thus, the presence of sediment and/or its thickness would not be a major factor in strongly influencing the nature and severity of shaking in the south-southwest region (MMI VIII sites).

Conclusions

We present the source parameters of the three earthquakes in Gyeongju, South Korea, on September 2016 with M_w exceeding 4.0 and discuss the relevance of these events with reference to seismic activities pertaining to the Yangsan fault system. The source mechanism of the foreshock,

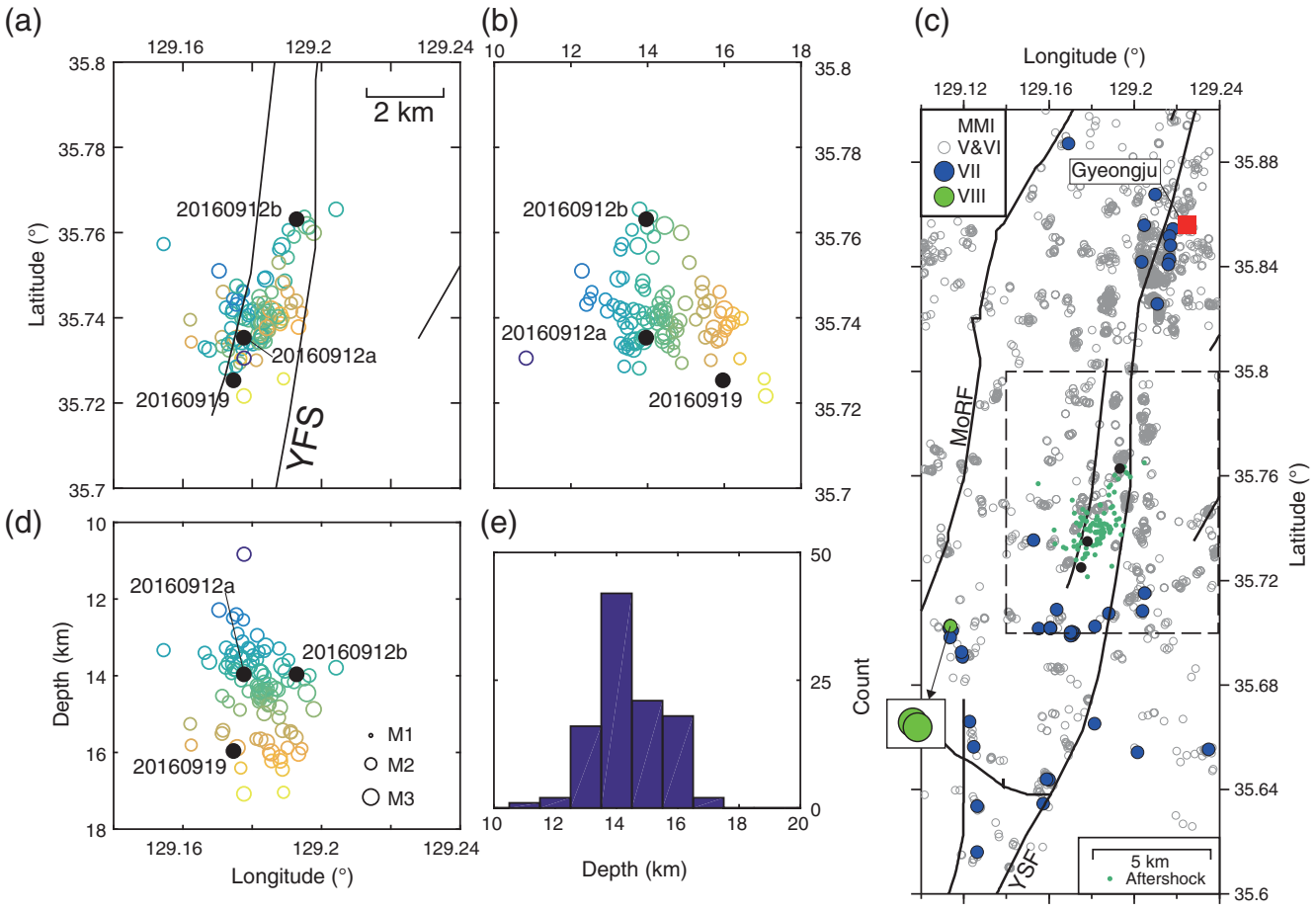

Figure 4. Distribution of aftershock earthquakes and modified Mercalli intensity (MMI) estimates. (a,b,d) Distribution of the 102 aftershocks for the period 12 September 2016 to 15 November 2016. The earthquake with $M_L < 3.5$ is indicated by an open circle, and three earthquakes (Table 1) are indicated by the black dots. (c) Map of the MMI intensity estimates (MMI = V–VIII). The region of (a) is indicated as a dashed box. Note that the MMI VII and VIII intensities are dominantly reported along the Yangsan fault system between the latitude of 35.6°–36.0°. In particular, we observe high intensities (MMI = VIII) in two sites south-southwest of the epicentral region. See caption of Figure 1 for abbreviations. (e) The depth distribution of the aftershocks plotted as a histogram.

mainshock, and aftershock events (M_w 5.1, 5.5, and 4.3, respectively) shows strike-slip motion on the fault system at a depth range of 14–16 km, based on the regional waveform inversion. The analysis results clearly show a preferred along-strike propagation direction of earthquake ruptures in the Yangsan fault system to the south-southwest. This rupture propagation direction agrees well with the spatial distribution of the relocated aftershock events for the period of about two months and the reported seismic intensities.

Data and Resources

Two sets of seismic data from the Korea Institute of Geoscience and Mineral Resources (KIGAM) and the Korea Meteorological Administration (KMA) are available with permissions at http://quake.kigam.re.kr (last accessed November 2016) and http://necis.kma.go.kr (last accessed November 2016), respectively. The earthquake catalog is obtained at http://necis.kma.go.kr (last accessed November 2016). Some of the figures are plotted by Generic Mapping Tools (Wessel and Smith, 1998). The codes for the Baysian Hierarchical Seismic Event Locator (Bayesloc) and hypoDD are from https://www-gs.llnl.gov/about/nuclear-threat-reduction/nuclear-explosion-monitoring/bayesloc (last accessed June 2014) and http://www.ldeo.columbia.edu/~felixw/hypoDD.html (last accessed March 2014), respectively. The Global Centroid Moment Tensor solution and the U.S. Geological Survey moment tensor solution are obtained by http://www.globalcmt.org (last accessed November 2016) and http://earthquake.usgs.gov/earthquakes/search/ (last accessed November 2016), respectively.

Acknowledgments

Y. Kim acknowledges the Korea Meteorological Administration (KMA) Research and Development Program under Grant KMIPA2015-7020. We thank KMA and the Korea Institute of Geoscience and Mineral Resource (KIGAM) for providing seismic-waveform data and local government officers of Gyeongju and Ulsan cities for their effort to survey damages. Finally, the authors thank Editor-in-Chief Thomas Pratt and reviewers for comments that significantly improved this article.

References

Chang, C., J. B. Lee, and T.-S. Kang (2010). Interaction between regional stress state and faults: Complementary analysis of borehole in situ stress and earthquake focal mechanism in southeastern Korea, *Tectonophysics* **485,** 164–177.

Chong, J., S. Ni, and X. Zeng (2010). *sPL*, an effective seismic phase for determining focal depth at near distance, *Chin. J. Geophys.* **53,** no. 11, 2620–2630 (in Chinese).

Chung, T. W., and W. H. Kim (2000). Fault plane solutions for the June 26, 1997 Kyong-ju earthquake, *J. Korean Geophys. Soc.* **3,** no. 4, 245–250 (in Korean with English abstract).

He, X., S. Ni, and J. Liu (2015). Rupture directivity of the August 3rd, 2014 Ludian earthquake (Yunan, China), *Sci. China Earth Sci.* **58,** no. 5, 795–804, doi: 10.1007/s11430-015-5053-2.

Jeong, G. Y., and C.-S. Cheong (2005). Recurrent events on a Quaternary fault recorded in the mineralogy and micromorphology of a weathering profile, Yangsan fault system, Korea, *Quaternary Res.* **64,** 221–233, doi: 10.1016/j.yqres.2005.05.008.

Jo, N. D., and C.-E. Baag (2003). Estimation of spectrum decay parameter k and stochastic prediction of strong ground motions in southeastern Korea, *J. Earthq. Eng. Soc. Korea* **7,** 59–70 (in Korean with English abstract).

Kim, S., J. Rhie, and G. Kim (2011). Forward waveform modelling procedure for 1D crustal velocity structure and its application to the southern Korean Peninsula, *Geophys. J. Int.* **185,** 453–468, doi: 10.1111/j.1365-246X.2011.04949.x.

Kim, Y., J. Rhie, T.-S. Kang, K.-H. Kim, M. Kim, and S.-J. Lee (2016). The 12 September 2016 Gyeongju earthquakes: 1. Observation and remaining questions, *Geosci. J.* **20,** no. 6, 747–752.

Klein, F. W. (2002). User's guide to HYPOINVERSE-2000, a Fortran program to solve for earthquake locations and magnitudes, *U.S. Geol. Surv. Open-File Rept.*, 35–39.

Kyung, J. B. (2003). Paleoseismology of the Yangsan fault, southeastern part of the Korean Peninsula, *Ann. Geophys.* **45,** no. 5, doi: 10.4401/ag-3465.

Kyung, J. B., and K. Lee (2006). Active fault study of the Yangsan fault system and Ulsan fault system, southeastern part of the Korean Peninsula, *J. Korean Geophys. Soc.* **9,** 219–230.

Lee, K., and Y. G. Jin (1991). Segmentation of the Yangsan fault system: Geophysical studies on major faults in the Kyeongsang basin, *J. Geol. Soc. Korea* **27,** no. 4, 434–449.

Ma, S. (2010). Focal depth determination for moderate and small earthquakes by modeling regional depth phases *sPg*, *sPmP*, and *sPn*, *Bull. Seismol. Soc. Am.* **100,** 1073–1088.

Ma, S., and G. M. Atkinson (2006). Focal depth distribution for earthquakes with $m_N \geq 2.8$ in western Quebec, southern Ontario, and northern New York, *Bull. Seismol. Soc. Am.* **96,** 609–623.

Myers, S. C., G. Johannesson, and W. Hanley (2007). A Bayesian hierarchical method for multiple-event seismic location, *Geophys. J. Int.* **171,** 1049–1063.

Myers, S. C., G. Johannesson, and W. Hanley (2009). Incorporation of probabilistic seismic phase labels into a Bayesian multiple-event seismic locator, *Geophys. J. Int.* **177,** 193–204.

Park, J.-C., W. Kim, T. W. Chung, C.-E. Baag, and J.-H. Ree (2007). Focal mechanisms of recent earthquakes in the southern Korean Peninsula, *Geophys. J. Int.* **169,** 1103–1114.

Qin, L.-B., S. D. Ni, W.-W. Chen, and Y. Luo (2014). A method of resolving earthquake rupture directivity with relative centroid location and its application to the 2008 Yingjiang M_s 6.0 earthquake, *Chin. J. Geophys.* **57,** 3259–3269 (in Chinese).

Um, S. H., H. I. Choi, J. D. Son, J. H. Oh, Y. H. Kwak, S. C. Shin, and H. S. Yun (1983). Geological and geochemical studies on the Gyeongsang Supergroup in the Gyeongsang basin, *Korea Inst. Energy Resour. Bull.* **36,** 124 (in Korean with English abstract).

Waldhauser, F., and W. L. Ellsworth (2000). A double-difference earthquake location algorithm: Method and application to the northern Hayward fault, California, *Bull. Seismol. Soc. Am.* **90,** 1353–1368.

Wessel, P., and W. H. F. Smith (1998). New, improved version of generic mapping tools released, *Eos Trans. AGU* **79,** 579.

Zhao, L.-S., and D. V. Helmberger (1994). Source estimation from broadband regional seismograms, *Bull. Seismol. Soc. Am.* **84,** 91–104.

Zhu, L., and L. A. Rivera (2002). A note on the dynamic and static displacements from a point source in multilayered media, *Geophys. J. Int.* **148,** 619–627.

School of Earth and Environmental Sciences
Seoul National University
Seoul 08826, Republic of Korea
younghkim@snu.ac.kr
hbim7676@snu.ac.kr
(Y.H.K., H.L.)

School of Earth and Space Sciences
University of Science and Technology of China
Hefei 230026, China
hexiaohu@mail.ustc.edu.cn
(X.H.H.)

CAS State Key Laboratory of Geodesy and Earth's Dynamics
Institute of Geodesy and Geophysics
Wuhan 430077, China
sdni@whigg.ac.cn
(S.D.N.)

Korea Meteorological Administration
Seoul 07062, Republic of Korea
suncheon@korea.kr
(S.-C.P.)

Manuscript received 4 January 2017;
Published Online 25 September 2017